Results in Engineering 25 (2025) 103781

Contents lists available at ScienceDirect

Results in Engineering

journal homepage: www.sciencedirect.com/journal/results-in-engineering

Detection of corrosion on silvered glass reflectors via image processing

Florian Wiesinger [a,*], Sarah Baghouil [b], Estelle Le Baron [c], Romain Collignon [c], Filipa Santos [d,e], Teresa C. Diamantino [d], Isabel Catarino [e], Jorge Facão [d], Cristina Ferreira [d], Soraia Páscoa [d], Florian Sutter [a], Aránzazu Fernández-García [f], Johannes Wette [f]

[a] German Aerospace Center (DLR), Institute of Solar Research, Calle Doctor Carracido Nr. 44, 1st Floor, 04005 Almería, Spain
[b] AGC Glass Europe, Rue Louis Blériot n°12, 6041 Gosselies, Belgium
[c] Univ. Grenoble Alpes, CEA, Liten, Campus Ines, 73375 Le Bourget du Lac, France
[d] Laboratório Nacional de Energia e Geologia, Estrada do Paço do Lumiar, n°22, 1649-038 Lisboa, Portugal
[e] LIBPhys-UNL, Department of Physics, NOVA School of Science and Technology, NOVA University of Lisbon, Portugal
[f] Centro de Investigaciones Energéticas, Medioambientales y Tecnológicas (CIEMAT). Plataforma Solar de Almería (PSA), Ctra. de Senés s/n km 4, Apartado 22, 04200 Tabernas, Spain

ARTICLE INFO

Keywords:
Round Robin
Concentrating solar power
Corrosion
Reflector qualification
Image analysis

ABSTRACT

A novel characterization technique based on image analysis is presented, intended to complement state-of-the-art reflectometer measurements. The technique is developed by experts from different laboratories (OPAC, AGC, CEA and LNEG), which subsequently conduct two Round Robin experiments on corroded solar reflectors for validation. Regarding the inter-comparability, it is found that parameters like the corrosion spot density or the penetration maximum on coated edges exhibit an average coefficient of variation of 62.6 % and 54.9 %. Better agreement is found for parameters like the total corroded area and the maximum edge corrosion penetration, with coefficients of variation of 14.3 % and 13.4 %, respectively.

The developed methodology is further applied during a 68-month lasting outdoor exposure campaign of two types of solar reflectors at two representative sites, one exhibiting corrosivity class C2 and the other C3. On the commercial coating RL1, a total corroded area of 59 mm^2 and 426 mm^2 is measured after the outdoor exposure on the C2 and the C3 site, respectively, while on the novel low-lead coated reflector RL3 corresponding values are 280 mm^2 and 1308 mm^2. This shows the superior quality of the coating RL1 in terms of corrosion resistance. Furthermore, the analysis highlights the importance of proper edge sealing for corrosion protection, since corrosion penetration is increased by a factor between 1.3 and 4.0 if the edges are unprotected. The reflectance decrease after the outdoor exposure is regarded as negligible (0.000 - 0.005), thus not permitting any of the conclusions that are made from the novel image analysis technique.

Acronyms

CIEMAT	Centro de Investigaciones Energéticas, Medioambientales y Tecnológicas
CST	concentrated solar thermal
CSP	concentrated solar power
DECORI	Detection of Corrosion via Image Processing
D&S	Devices and Services reflectometer
MED	multi-effect distillation
OPAC	Optical Aging Characterization Laboratory; a joint laboratory between CIEMAT and DLR at PSA
PSA	Plataforma Solar de Almería owned by CIEMAT
PV	photovoltaic

(*continued on next column*)

(*continued*)

Symbols

A	absorptance [-]
CV	coefficient of variation [%]
I	brightness of pixel, value between 0 and 255 [-]
Λ	wavelength [nm]
Φ	acceptance half-angle [mrad]
P	reflectance [-]
$\rho_{s,h}$	near-normal solar-weighted hemispherical reflectance [-]
$\rho_{\lambda,\varphi}$	near-normal monochromatic specular reflectance [-]
θ_i	incidence angle of reflectance measurement [°]

* Corresponding author.
E-mail address: florian.wiesinger@dlr.de (F. Wiesinger).

https://doi.org/10.1016/j.rineng.2024.103781
Received 8 November 2024; Received in revised form 10 December 2024; Accepted 18 December 2024
Available online 24 December 2024

1. Introduction and motivation

Concentrated Solar Thermal (CST) technology is used to harness solar energy for electricity and heat generation. Central to the success of CST systems are solar reflectors, which concentrate sunlight onto a receiver to produce high-temperature heat. The investment cost of solar reflectors represents around 6.4 % of the initial investment of a typical Concentrated Solar Power (CSP) plant [1]. It is of crucial importance for the plant owners that the optical performance of the reflectors remains at a high level throughout their service lifetime, aimed at 25 years and more [2]. Usually, silvered-glass reflectors are employed for CST technologies due to their excellent optical performance and high durability. They have proven their resistance to environmental effects in many long-term exposure projects [3] and reflectors from the 80's are still partially in operation in the SEGS power plant. However, the omnipresent urge to lower production costs forces manufacturers to produce more economic materials. Also, new restrictions (low-lead- or lead-free paint compositions [4]) from governments or supranational organizations limit the production of well-proven material compositions, on the other hand this gives also rise to novel approaches like Njoku et al. who use expired drugs as corrosion inhibitors [5]. Hence, the market always offers new reflector compositions which still have to be tested regarding their environmental resistance and durability. Furthermore, new CST plants are increasingly projected at sites where harsh environmental conditions are present, like in desert areas or in close proximity to the sea. The later ones are utilized for water desalination applications, called CSP + MED (multi-effect distillation) and need to be located near to the coast [6,7]. These locations represent higher durability demands for the utilized plant components.

The durability is threatened by various meteorological and geological factors which can potentially lead to performance losses, e.g. humidity, thermal gradients and cyclic day-night temperature changes, irradiation, corrosive atmospheres, mechanical wear etc. To simulate outdoor effects on reflector surfaces, accelerated aging tests are applied under laboratory conditions with the aim to provoke similar failure mechanisms in considerably shorter times [8]. Corrosion has been identified as one of the main degradation mechanisms which might affect the durability and the optical behavior of solar mirrors [9]. Additionally, some places such as the Atacama Desert reported corrosive environments at night provoked by a sea fog, called "Camanchaca", which penetrates into the desert during some periods of the year [10]. Also, there are some CST plants already built near the sea where corrosion issues could appear in the future. For instance, Noor Energy 1 PSC (Dubai) is situated around 50 km from the sea in air-line distance. In all these situations, reflectors will be subjected to harsh corrosive environment, and it is vital to study their durability in order to predict the proper performance of the CST system and anticipate corrective measures during the installation, operation and maintenance. The ISO standard 9223:2012 [11] was established to determine the corrosivity classification of a certain outdoor site. The standard stipulates the outdoor exposure of four standardized metal coupons which are analyzed in the laboratory after one year focusing on their weight loss. This analysis is performed following a specific treatment to remove oxidized components on the different coupons. It is oftentimes used and representative results can be seen in literature [12–14]. A recently published work presents the varying intensity of corrosion effects emerging on silvered-glass solar reflectors exposed at different outdoor sites representing those corrosivity site classes [15]. Reflectance is the most important optical parameter for evaluating reflector efficiency in solar energy applications, and it is a major criterion for assessing their degradation [16]. The best standardized technique for calculating near-normal solar-weighted hemispherical reflectance, $\rho_{s,h}$ uses spectrophotometric measurements with an integrating sphere to determine the hemispherical reflectance at each different wavelength, λ in the range of 320 nm to 2500 nm, over the whole solar spectrum. Another important parameter to qualify solar reflectors is the near-normal monochromatic specular reflectance $\rho_{\lambda,\varphi}$ which describes the fraction of the reflected beam that reaches the receiver aperture under a representative acceptance half-angle φ. For more details on optical characterization methods on solar reflectors see e.g. the Solar Paces Guideline [17], Fernández-García et al. [18] or Sansom et al. [19]. However, both measurement techniques exhibit the disadvantage of accounting only for a very limited spatial area. The measurement spot usually only spans a few square centimeters on samples that are typically 10 cm x 10 cm. Since corrosion represents a local phenomenon that easily surpasses these dimensions, its properties like actual size and growth rate cannot be qualified by traditional reflectance measurements, which hence lack the possibility of an early detection and quantification of this common degradation phenomenon. Therefore, an image analysis technique has been used in a recent study by Buendía-Martínez et al. [15]. Their group established a lifetime prediction of novel coating compositions for solar reflectors. It was facilitated by comparing the outdoor achieved data with accelerated aging experiments through the assessment of their image analysis algorithm. However, the results of the image analysis were limited to the single parameter of total corroded area. No distinction between central and edge corrosion was made, and also no more details about the corrosion spot characteristics were determined. Given the significance of their findings for the development of novel coating compositions, a more comprehensive and extensive application of their analysis methodology is of interest which shall be done in the here presented work. A study undertaken by Khayatazad et al. [20] also uses image analysis to detect corrosion on steel structures. They were able to efficiently find corroded areas in digital images of large industrial assets. Hence, their accuracy demands were different than in the here presented work. They optimized their methodology also for faster processing time, and pixel dimensions are in the range of centimeters, while in the here presented work, time was not a constraint and pixel dimensions were in the micrometer range. Another group around Forkan et al. [21] offers a similar approach to the corrosion detection issue. Both works justify the methodology to be applied for the current case of solar reflectors as well.

Similar image based approaches were also used in the field of solar energy to forecast the power output of solar energy applications [22] and furthermore on soiling effects on solar reflectors. In the work of Smestad et al. [23], the participating authors answered the crucial questions about the intrinsic accuracies and comparabilities of the applied methodologies for soiling detection via image analysis. From the results of eleven participants they deduced that the coefficient of variation of parameters like the fractional area coverage of sand particles was 35 %, the value for the mean particle size was 15 % and the value for the number of particles could be over 80 %. Two main conclusions were then formulated. First, due to a lack of a standard methodology and a suitable reference image, the image analysis is subject to significant uncertainty. The results of micrograph-based soiling characterization can vary depending on the operator, even if the same image and the same processing software are employed. Furthermore, a particular image analysis procedure might give a reasonable variability for one micrograph, but may give a larger variability for another. The required procedure may need to be modified. The second conclusion, however, is that it was found that some parameters are less variable than others, and therefore more robust to image analysis. This opens the possibility to the discovery of other parameters that would be useful for comparing results across various laboratories and studies. Those two conclusions motivated the current work for a commonly accepted and standardized methodology and for the joint search for robust and reasonable parameters of comparison.

In another work on the soiling topic, Micheli et al. [24] analyzes the robustness of various thresholding methodologies integrated in the software ImageJ. They could find significant differences in the resulting parameters after analyzing 13,200 micrographs. The method with the lowest coefficient of variation was also one of the methods that were most often selected as best by the eleven human operators. Their work

points out that additional studies are needed to evaluate the accuracy of the various image analysis methods and to further contribute to identifying best practices for soiling estimation via this methodology.

The mentioned works have shown to deliver reasonable results, but for the methodology to be applied at a broader scale, the determination of its intrinsic accuracies and the comparability between different institutes has yet to be checked on.

This paper presents a novel algorithmic approach for the analysis of images taken from solar reflectors, enabling the precise detection of corroded areas and the quantitative assessment of corrosion progression over time. Results are obtained from four groups of experts on the same reflector samples and are compared among each other in the form of a Round Robin to assess the uncertainties of the presented approach. It should be highlighted that this work does not aim to identify the accuracies of the various methods, but rather to raise awareness on the potential dissimilarities that can be generated by different operators performing an analysis of the same samples.

2. Methodology

The here presented work is divided into three sections: first, an initial Round Robin test is conducted among four participants: The OPAC laboratory (joint collaboration between the German Deutsches Zentrum für Luft- und Raumfahrt (DLR) and the Spanish Centro de Investigaciones Energéticas, Medioambientales y Tecnológicas (CIEMAT)), AGC Glass Europe (AGC), Commissariat à l'Énergie Atomique et aux Énergies Alternatives (CEA) and Laboratório Nacional de Energia e Geologia (LNEG). Therefore, three different corroded samples were sent around, and each participant had the task of determining the corroded area quantitatively via image analysis. Every participant built their own setup and evaluated their acquired images independently. Afterwards the results were compared.

Based on the experience gained in the first Round Robin, parameter definitions were clarified, and analysis methods were optimized among the participants. These improvements are presented in detail in the second section of the paper. Also, a second Round Robin was performed with a new batch of five corroded samples that was sent around between the participants to benchmark their optimized analysis method.

In the third section, the developed technique was applied to images taken of reflector samples from long time outdoor exposure experiments during the H2020 Raiselife project in different sites of the world, which have been classified regarding their corrosion severeness [15].

2.1. Materials and reagents

The samples that are analyzed in this project are silvered float-glass reflectors with high technical performance to be used in concentrating solar technologies. The sample size is 10 cm x 10 cm and samples exhibit a thickness between 1 mm and 4 mm. The edges of the samples are either original (grinded/coated) edges or unprotected (cut) edges. The technique is aimed to evaluate changes in the silver layer and consequently all other alterations of the sample shall be avoided i.e. damages of the glass surface cannot be present. The sample needs to be a square and cannot have any cavities on its edges or chipping of the glass on the corners, this would lead to an incorrect overestimation of corrosion. Also, the sample has to be cleaned before the image is taken. Compressed dry air (free of particles and oil) shall be applied. In case of remaining dust or soil, demineralized water, a mild detergent, and a soft tissue can be employed. Abrasive or dissolvent agents that may change the properties of the sample shall never be employed by total immersion. Acetone might be used to ensure that any type of dust or fingerprints are totally removed. The acetone must be strictly applied on the glass surface with a soft tissue, avoiding contact with the backside of the sample and the edges.

Samples shown in this work emanate from outdoor exposure or accelerated laboratory aging tests [25–27]. Details on the exposure/accelerated testing are not part of this work, please refer to the respective literature. This work shall focus on the image-based analysis technique and describe the methodology which is used to derive quantitative corrosion parameters for the IEC standard PT62862–3–6 dealing with the durability of silvered glass reflectors, which is to be published soon.

2.2. Round Robin testing of corrosion detection

In order to get a first idea on possible difficulties regarding the comparability of the results from different laboratories and setups, a Round Robin was performed on three corroded samples coming from artificial aging experiments at OPAC. For this first Round Robin, there was only a limited amount of instruction given to the participants in order not to bias the understanding of this phenomenon and how it should be treated. Since there is no standard developed so far and resulting parameters are to a certain extent operator dependent, a wide range of interpretations is welcome at this stage. For the second Round Robin however, the definitions were more precise, and the lessons learnt from the first Round Robin were implemented in order to have more consistency between the participants and especially a more reasonable evaluation from a physical point of view. For the reproducibility of the results, the image acquisition process is of crucial importance. Stable conditions are required to ensure that the quality and the key elements that shall be extracted from the image are not altered or disturbed by any environmental effects during the image acquisition. Typical conditions that shall remain constant during the acquisition of various images for different samples are the illumination, the perspective, camera settings like ISO or shutter speed and the distance between the sample and the camera. The different setups which were built for the image acquisition at the four institutes are explained in the following subsections.

2.2.1. Setup at OPAC

The photo box which is displayed in Fig. 1 is based on an earlier prototype developed in the OPAC laboratory by Sutter et al. [28]. It contains the following elements: The single lens reflex camera D850 from the company Nikon (Tokio/Japan), exhibiting a resolution of 45.7 megapixels, equipped with a Micro Nikkor objective with a focal length of 105 mm and an aperture of 1:2.8, also from the company Nikon. The images were taken with the settings that are displayed in Table 1. It shall be stated, that these values result in reasonable images for the here presented setup and do not represent absolute values for other setup conditions. However, the following guidelines shall be followed when camera settings have to be selected for a setup:

- No overexposure of pixel shall occur in the reflective parts of the sample. Hence, illumination and shutter speed have to be adapted accordingly. After converting the image to greyscale, no pixel should have a value of brightness of 255.
- No compression or conversion of the raw image data shall be applied by the camera or the image taking software.
- The distance between the camera and the sample is selected in such a way that the sample area covers as much of the image as possible to increase the resolution in pixels of the sample area.

The sample is always placed in the exact same position and orientation towards the camera. Therefore, a special sample holder was constructed. It includes a vacuum pump which ensures the perfectly upright position of the sample. Furthermore, the sample holder allows the photographing of the sample with a certain, always constant background of green color. This is necessary for an accurate object detection mechanism which distinguishes between background and actual sample. As it is displayed in Fig. 1 on the right side, the surface normal of the sample is slightly rotated away from the vector between sample and camera. Hence, an image of the white screen is taken instead of a reflex of the camera itself. The box also contains a LED light source to provide

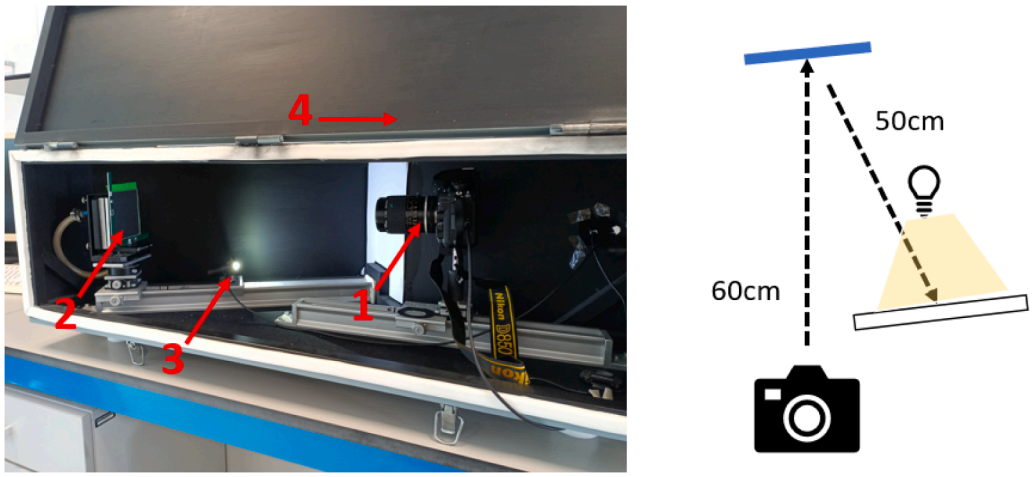

Fig. 1. Left: photo box setup exhibiting the following components: 1) Nikon D850, 2) reflector sample, 3) LED light source and 4) lid to close the box. Right: illustration of the image taking process seen from the top.

Table 1
Camera Settings for the D850 during the image acquisition.

Parameter	ISO	Shutter Speed	Image Format	Compression
Value	250	1/2 s	TIFF	Uncompressed RAW

homogeneous and stable illumination conditions once the lid is closed for the image acquisition process. Note that the LED is not directed towards the sample but to the white screen which reflects the light in a diffuse way. The LED is powered by an LED driver providing a stable and reproducible intensity.

2.2.2. Setup at AGC

Pictures and an illustration of the photo box built by AGC are given in Fig. 2. Every material inside the box except for the white reflected material and the green background behind the reflector sample (not shown on the picture of Fig. 2) are black colored. There is also a black sliding lid that closes the upper side of the box and the box itself is located in a black room.

The reflex camera is EOS 100D from the company Canon (Tokio/Japan), exhibiting a resolution of 18 megapixels, equipped with an EFS objective with a focal length of 45 mm, also from the company Canon. The images were taken with the settings that are displayed in Table 2.

The camera takes a picture of the reflector sample that is reflecting the image of the white material located in front of it. Both the camera and the sample are tilted from the vertical plane so that the camera does not capture a reflection of itself. The reflector is illuminated with two LED sources located above and below it. The drawback is that the sample is not uniformly illuminated because of the shadows of the sample holder and of the thickness of the sample itself. A way to optimize this

Table 2
Camera Settings for the EOS 100D during the image acquisition.

Parameter	ISO	Shutter Speed	Image Format	Compression
Value	100	1/4 s	JPG	Uncompressed RAW

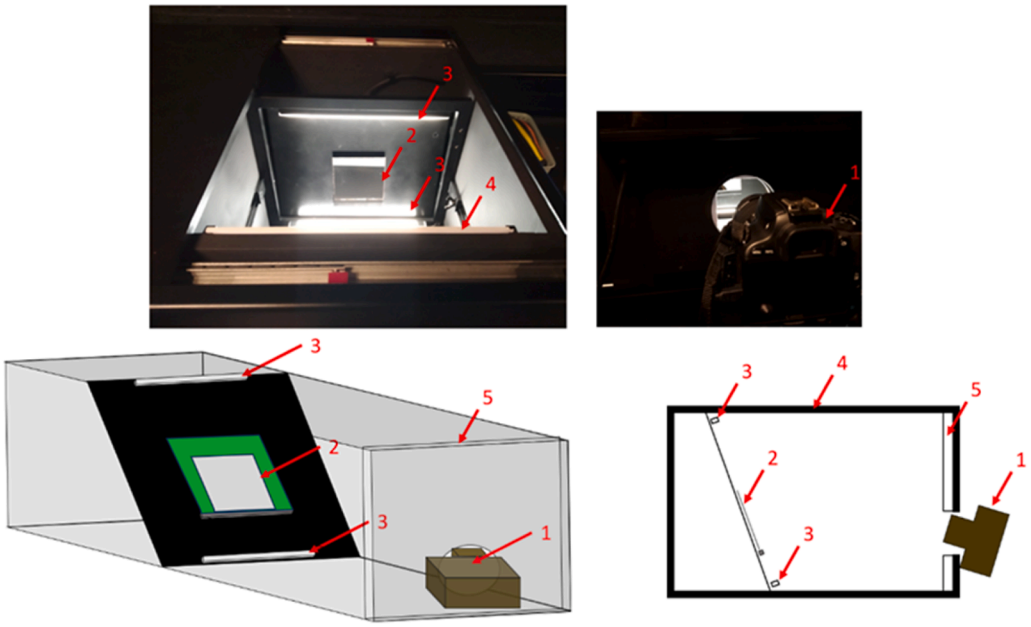

Fig. 2. Top: photo box setup exhibiting the following components: 1) Canon EOS 100D, 2) reflector sample, 3) LED light sources 4) lid to close the box and 5) white reflecting material. Bottom: illustration of the image taking process.

setup is to illuminate the white reflected material through one light source. A green background is placed behind the sample, which was found to be more adapted than a black background in order to differentiate the sample from its background.

2.2.3. Setup at CEA

The absence of reflection is required to ensure a good quality of the image acquisition. So, CEA decided to place the reflector on different colored papers which makes it easy to delineate the edges of the mirror in a photo bench which is in a dark room. This is necessary for an accurate object detection to distinguish the background and the sample.

A large white sheet (minimum A3 format) is placed horizontally above the mirror at 60 cm distance. The smartphone can be fixed on a support or as in the photo with a minimum angle to see the reflection of the mirror in the white paper but also to avoid being in the angle of reflection. Two lamps, placed on either side of the white paper illuminate the mirror.

The perspective conditions remained constant during the acquisition of the different images for different samples between the sample and the camera. To fulfill all these requirements, a smartphone mounting bracket is suitable.

Fig. 3

The scope is to perform simple photography without sophisticated camera nor box only a simple smartphone. The following guidelines shall be followed:

- No reflective parts of the sample should be photographed (the entire mirror must reflect on the white paper).
- Sufficiently large and homogeneous illuminations from different orientations are needed to avoid lateral shadows. The lamps are directed towards the sample from a large white paper.

The distance between the camera and the sample is selected in such a way that the sample area covers as much of the image as possible to increase the resolution in pixels of the sample area.

2.2.4. Setup at LNEG

In the apparatus built at LNEG, a Panasonic Lumix DMC-G7 camera with a resolution of 16 megapixels equipped with the Lumix G Macro 30 mm f/2.8 lens and the corresponding camera support were used. The photographs were taken under the following conditions:

Parameter	Aperture	Shutter Speed	Image Format	Compression
Value	3.2	1/125	JPEG	Compressed JPEG

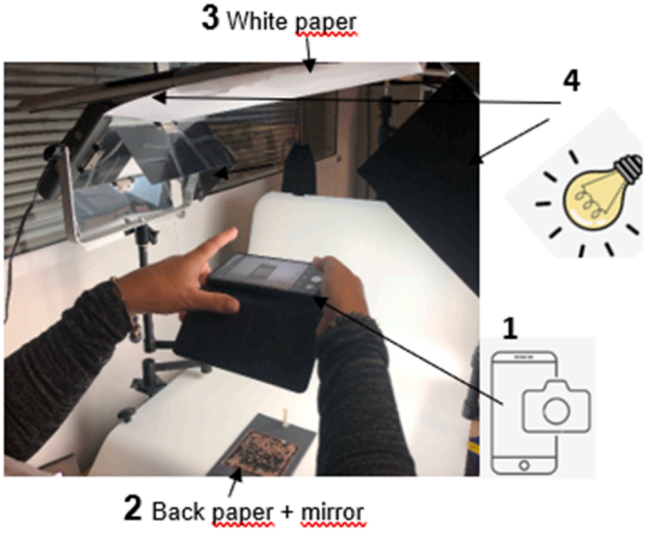

Fig. 3. Image taking setup exhibiting the following components: 1) smartphone, 2) mirrors on a black paper, 3) white paper and 4) two lamps.

A strip of LED tape placed on the ceiling of the box where the setup is mounted ensures a homogeneous distribution of light through the white diffusers placed on both the back wall and the door of the box. The samples are attached to the holder with adhesive paste. The front of the holder - the one facing the camera - is colored green, a feature that improves the detection of sample boundaries. To ensure that the sample is properly placed in the holder, the latter is taken off every time a different sample is to be photographed and then put back on with the sample. Since the position and the direction of the holder are predefined on the metallic guides where it is placed, only minor adjustments of the direction of the sample holder are required in order to get the best photo.

Considering that the samples to be photographed are solar reflectors, it was necessary to direct them slightly towards the white diffuser, so that the reflection of the white could be captured and not that of the camera reflection.

Fig. 4

2.2.5. Image treatment - OPAC

The following section describes the workflow of the DECORI (Detection of Corrosion via Image Processing) algorithm, developed by OPAC from the raw images to the final extraction of the parameters of interest. The code is written MATLAB. Each subsection gives an exemplified illustration of the particular image treatment process.

Step 1: sample detection

The image in its initial form can be seen in Fig. 5a). It is taken of a sample in its as-received state i.e. without any defects and corrosion spots. This sample will be used as a reference sample with respect to the aged samples. As a first step, the extraction of the relevant area of the image is required. Therefore, a conversion of the color space from RGB to HSV is performed and all the pixels of green color are segmented. All the other pixels are displayed in black color in Fig. 5b) to illustrate the process. From there on, the largest non-green tetragon is classified as the complete sample area. The respective corner points and edges of this tetragon are marked in red in the initial image as it can be seen in Fig. 5c).

Step 2: transformation

The four corner points from step 1 are used to perform a geometric transformation of the initial image to a quadratic image of the side length of 10 cm. For the application in the algorithm this absolute length has to be converted into a pixel length by a conversion factor which depends on the geometry of the setup. In the here presented setup configuration the conversion was 10 cm equal 4770 pixels. This also represents the final resolution of the evaluated sample which is 20 μm per pixel.

Due to the camera perspective and the slight horizontal tilting of the sample, certain artefacts can be seen on the edges of the sample. This is especially the case, if grinded edges are present on the sample. This results in a grey area on the right side of the reflector as it is indicated by the arrow in Fig. 6b). It is important to identify such artefacts on the reference sample since they will reappear on the aged samples as well, and shall not be detected as corroded areas there.

Step 3: thresholding

The first two steps are carried out on the reference sample and the aged sample, which is to be subjected to subsequent analysis (see Fig. 7a)). Then, both resulting RGB images are converted to grayscale in order to obtain the scalar value of pixel intensity I between 0 and 255 for every pixel. Afterwards a pixel by pixel division is carried out to obtain the brightness ratio between the aged - and the reference grayscale image. The resulting representation of this ratio I_{aged} / I_{ref} can be seen in Fig. 7b). Where the value is close to 1, aged - and reference image exhibit the same brightness and hence no corrosion is present at these pixels. For pixels with values smaller than 1 however, the brightness of the aged sample is lower than for the reference. Areas which are displayed in blue color can be understood as completely corroded and the corresponding

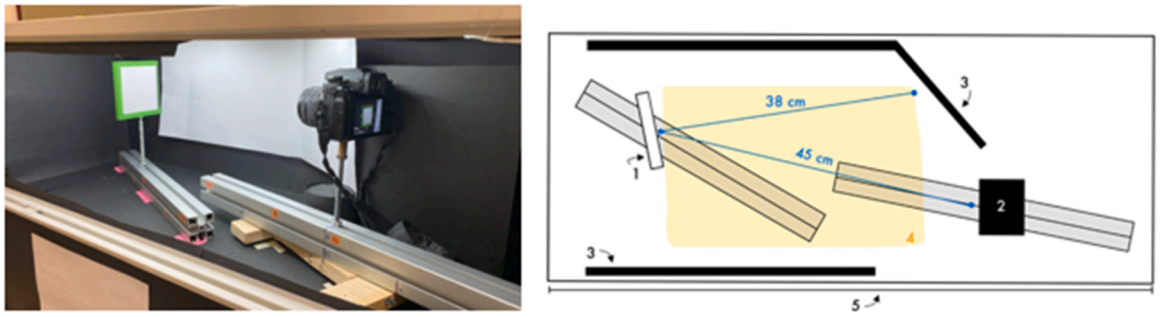

Fig. 4. Left: photo box setup from LNEG. Right: schema of the image capturing setup as seen from the top and exhibiting the following components: 1) Sample holder, 2) Panasonic Lumix DMC-G7, 3) Light diffuser, 4) LED light source and 5) Lid to close the box.

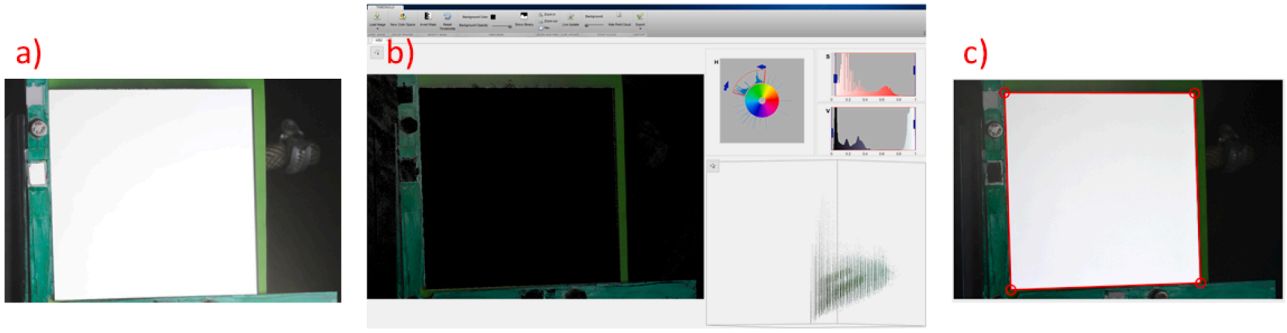

Fig. 5. Illustration of step 1, the accurate sample detection: a) initial image taken with the setup in the OPAC laboratory, b) segmentation of the green parts of the image and c) cropping of the inner area of the green background.

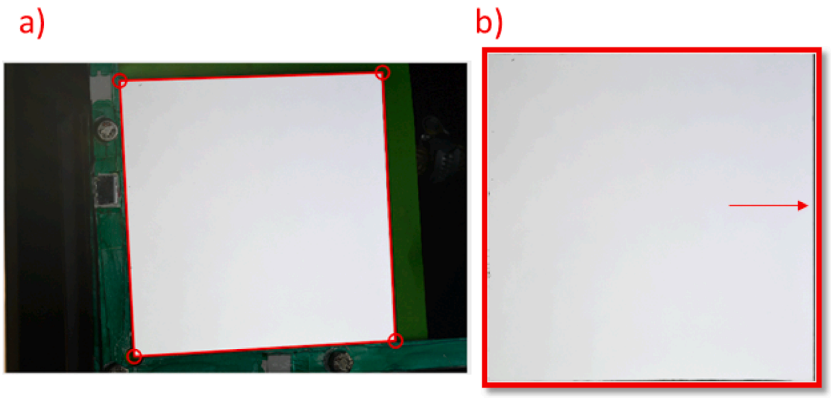

Fig. 6. Illustration of step 2: geometric transformation from tetragon to square: a) image of sample in sample holder with the four corner points marked, b) sample area transformed to perfect square of 10 cm length (red frame here only for illustration to separated image from paper/screen background). Arrow indicates artefact from sample tilting.

pixels do not contribute to the reflection of sunlight in a significant way anymore.

At this point, it is important to note that a direct evaluation of the grayscale image of the aged sample without the reference image would not lead to the same meaningful results. The acquired results would always be highly depending on the illumination conditions and camera settings, they could hardly be reproduced in another setup/laboratory and present artefacts could not be separated from corrosion. Therefore, it is of major importance to work with brightness ratios based on the intact brightness for every pixel. The ratio I_{aged} / I_{ref} is also displayed in a histogram in Fig. 7c). A reasonable threshold value to differentiate between an intact/reflective pixel and a corroded one is certainly lying in the range of 0.85 and 0.95, which is marked by the orange area in the histogram. A comparison between the resulting corroded area after the application of a threshold of 0.93 and images taken by an optical microscope of the same corrosion spots can be seen in Fig. 7d)-f). Because of the reasonable agreement in geometrical features and size, the value of 0.93 was used from now on as threshold.

Step 4: object postprocessing

The application of the thresholding rule constructs a binary image with black corroded objects and white reflective pixels. Several operations are then performed on the binary image which are explained in short.

connection of close objects: Corrosion on the edges of the sample is often observed to occur via the following process. First a thin line of corrosion forms starting from one point of the edge, penetrating into the sample and then connecting back to the edge at another point, thus encircling a certain area of the sample. The enclosed area still exhibits a

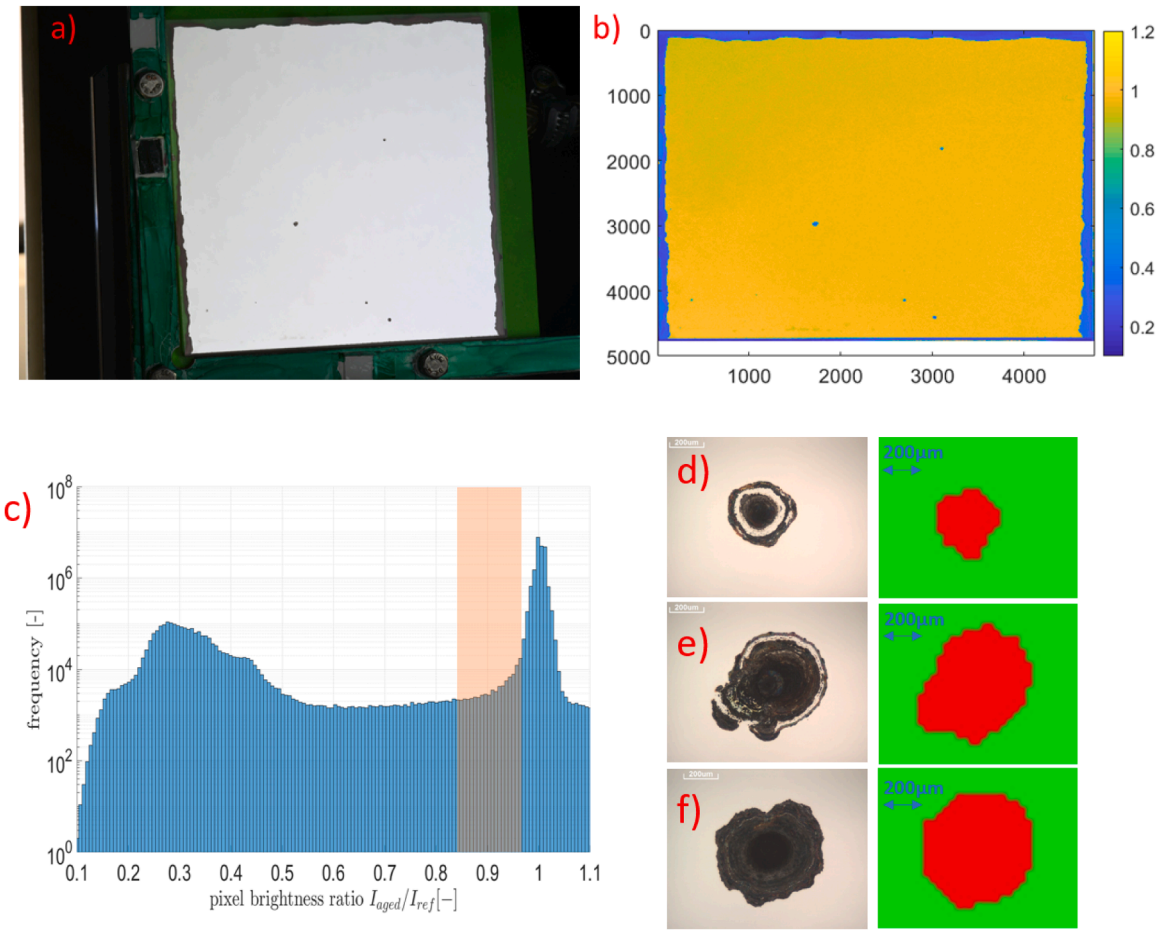

Fig. 7. a) raw image of aged sample, b) representation of pixel brightness ratio Iaged / Iref and c) histogram representation of I_{aged} / I_{ref}. The orange area between 0.85 and 0.95 marks the reasonable threshold values, from which on a pixel is identified as corroded or intact. d)-f) comparison between microscope images and results from image analysis with a threshold of 0.93.

high reflectivity at first, but very soon is corroding as well and hence this area shall be considered as corroded in the evaluation process. Examples of this phenomenon are seen in Fig. 8b) indicated by the arrows. To convert those enclosed white areas to black areas and also connect spots which are close to the edge corrosion area the command imclose is used. It performs a morphological closing on the binary image, using a disk of 20 pixels diameter as structuring element. The morphological close operation is a dilation followed by an erosion, using the same structuring element for both operations. After this operation, one connected and void-free edge corrosion area is achieved as it can be seen in Fig. 8c). Since this operation acts on the complete sample, it also merges single black objects in the inner area which are close to each other and should be treated as one large corrosion spot instead of many small ones which are in close proximity.

defect size segmentation: Regarding the size of the inner corrosion defects the following two conventions are adopted: The minimum equivalent defect diameter is 200 µm for an object to be detected as a corrosion spot. The imclose command from the earlier step merged many of those small objects already with larger objects in their vicinity. Now, remaining black objects are segmented if they exhibit less pixels

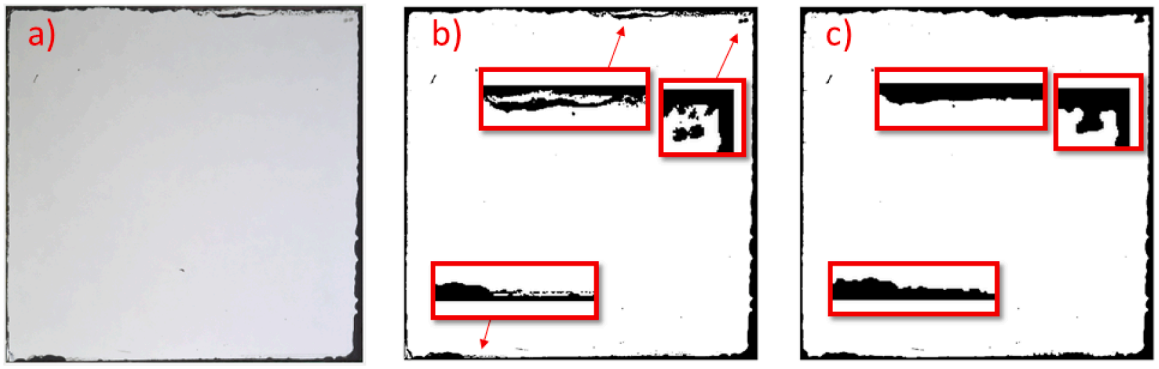

Fig. 8. Illustration of postprocessing step imclose: a) raw image of aged sample, b) corresponding binary image after the application of steps 1–3 with arrows and zoomboxes marking the critical areas that are treated in this step and c) resulting binary image with connected objects.

than a circle of 200 μm in diameter. Oftentimes this removes loosely adhering dust particles on the surface. The bwareaopen command is used for this step. The same process is applied for the maximum corrosion spot size. Therefore, spots with more pixels than a circle of 1000 μm in diameter are detected. Those objects however are not removed from the evaluation, they are just counted and their number is reported afterwards, since according to the IEC standard PT62862 the respective samples with corrosion spots lager than 1000 μm in diameter do not pass the acceptance criterium.

Step 5: determination of edge penetration

Another parameter of interest to qualify the corrosion severeness, is the progress of the advancing edge corrosion towards the inner area of the sample. The edge corrosion penetration is defined as the maximum distance between the edge and the corresponding edge corrosion pixels. In certain cases, it is not straightforward to assign a corroded pixel explicitly to one of the four edges. For the upper edge in the example shown in Fig. 9, it is pretty clear that the maximum penetration is going to be found in the middle area. For the other three edges however, this problem cannot be solved via a similar approach. An elegant way to assign each pixel to an edge is to find the largest inscribed rectangle of the inner area. This rectangle, illustrated by black dashed lines is displayed in Fig. 9b) and touches the corroded area of each edge at its maximum penetration point. The distance of each of those points to its corresponding edge is determined and the point is also marked in the image with a triangle. In addition to the maximum edge penetration also the mean edge penetration can be calculated. Therefore, those lines which are perpendicular to the respective edge are prolonged to limit the area where the mean penetration is calculated. This is exemplified for the upper edge by the double horizontal arrow.

Furthermore, it shall be noted that the sample shown in Fig. 9 exhibits one original edge on the right side, while the rest of the edges are cut and hence offer less corrosion resistance. It is of crucial importance to differentiate between those two edge types. However, this input is needed from the operator and the triangular maximum penetration points are displayed in orange and blue color for cut and original edges, respectively.

Step 6: final image and data extraction

In the fifth step, the final image is constructed with all its color markings that are explained in the following using the example in Fig. 10. The thin red lines on the edges, particularly on the bottom edge, are indicative for the artifacts resulting from shadows and grinded edges. These red areas are not considered for any corrosion analysis. The light green area is the edge corrosion which is clearly less pronounced on the original bottom edge than on the cut edges. The inner corrosion spots are marked in dark green color and the maximum edge penetration points are marked with a triangle as it is explained in step 4.

Together with the image in Fig. 10b) which is useful for the operator to check if the DECORI algorithm did work in a proper way, the parameters of interest are exported in a table as it can be seen in Table 3. The different parameters are explained in the following:

sample name: This is the same name as the image input file has.

total corroded area [mm²]: The area of all pixels below the threshold in mm², excluding the shadow of the sample (red markings in the image). Inner corrosion spots (dark green) and the edge corrosion (light green) are counted.

corrosion spot area [mm²]: Only inner corrosion spots (dark green) are counted. As inner corrosion spots, only objects with an equivalent diameter of 200 μm are considered, all smaller objects are omitted.

spot density (intact area) [spots/cm²]: This parameter represents the *number* of inner corrosion spots over the area which is not affected by edge corrosion.

inner corrosion (intact area) [%]: This parameter represents the *area* of inner corrosion spots over the area which is not affected by edge corrosion.

max penetration coated [mm]: The maximum penetration of the edge corrosion for all the coated/original edges. The four maximum penetration points (one per edge) are marked in the image with a triangle (color is blue for coated edges).

mean penetration coated [mm]: The mean penetration of the edge corrosion for all the coated/original edges.

max penetration uncoated [mm]: The maximum penetration of the edge corrosion for all the uncoated edges. The four maximum penetration points (one per edge) are marked in the image with a triangle (color is orange for uncoated edges).

mean penetration uncoated [mm]: The mean penetration of the edge corrosion for all the uncoated edges.

spots ≥1 mm: Gives the number of spots in the inner area whose equivalent diameter is larger than 1 mm.

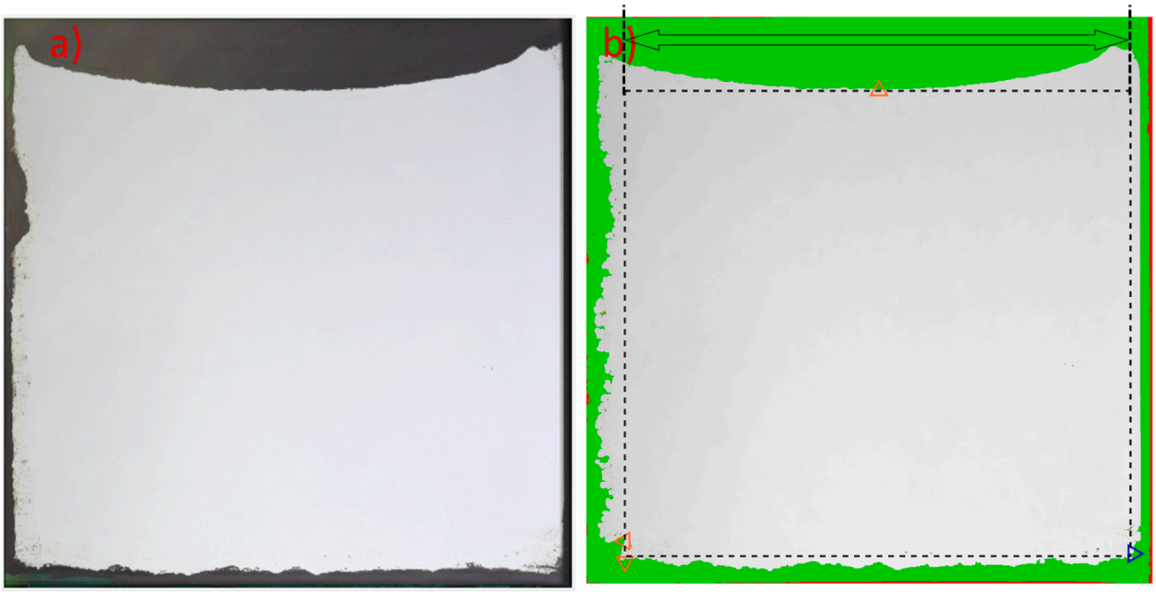

Fig. 9. Illustration of step 4, the edge penetration determination: a) transformed raw image of aged sample and b) evaluated image with largest inscribed rectangle and maximum edge penetration markings for each of the four edges in the form of a triangle are added. Left and right rectangular edge is prolonged upward to illustrate the horizontal distance where the mean edge penetration is evaluated.

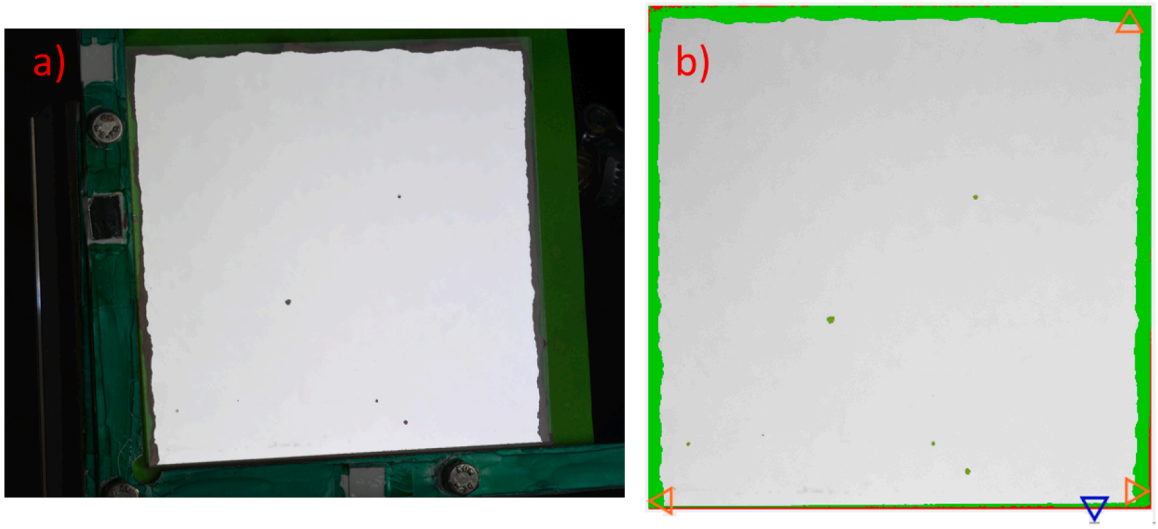

Fig. 10. comparison between a) initial raw image and b) evaluation result with all color markings applied.

Table 3
DECORI result table.

sample name	total corroded area [mm²]	corrosion spot area [mm²]	spot density (intact area) [spots/cm²]	inner corrosion rate (intact area) [%]	max penetration coated [mm]	mean penetration coated [mm]	max penetration uncoated [mm]	mean penetration uncoated [mm]	spots >1 mm
example.tif	799.66	4.6	0.09	0.05	0.42	0.18	2.79	2.55	2

2.2.6. Image treatment – CEA

The following section describes the image processing developed at CEA. The code is written in Matlab language. The process of obtaining results from the pictures can be described by the following three steps.

Step 1: Image transformation

Because the pictures are taken using a cell phone over the mirror, even with utmost care, the perspective has to be corrected. At the same time, the image can be cropped to remove any pixel that is not part of the mirror. Of all the subset of tested colored papers, the black sheet provided the best contrast between the background and the mirror. Enabling an easy discrimination between the white image reflected in the mirror or the brown from the corrosion. After converting the pictures to grayscale and normalizing the intensity values of every pixel between 0 and 1, it becomes apparent that a threshold of 0.6 discriminates very well between the object and the background. This step enables to determine the border of the mirror in the picture as well as its centroid.

The distance between the centroid and the border of the mirror can thus be evaluated for every pixel of the perimeter. This enabled to automatically determine the four corners of the mirror in the picture by finding local maxima of the centroid-perimeter distance. Finally, because the locations of the corners are known, the mirror from the photo can be morphed to a square of size the longest of the original in pixels. The interpolation is performed using the fitgeotrans function of Matlab.

Step 2: Threshold detection

At this point, the picture is a square normalized grayscale image of the mirror corrected from perspective deformation, where the black background of the photo was cropped. To discriminate between corroded and un-corroded pixels, the correct procedure has to be chosen. Advanced methods could be used, based on gradient or laplacian and edge detection, but a simple intensity threshold method works well in this case. To determine the best value for the threshold, the intensity distribution of the pixels in the image is calculated. Two well-separated normally distributed populations are highlighted. Thus, the threshold value chosen is the value where the distribution is minimum.

Step 3: Post-Processing

Thanks to the threshold value, two binary masks are obtained: the first highlights all the corroded pixels and the second which highlights only the corroded borders. The properties of each individual connected object in the image evaluated are: pixel list, centroid and area. This allowed to discriminate whether or not each object has a size over 200 μm or 1000 μm and evaluate the different results parameters.

To evaluate the penetration of the corrosion at the edges of the mirror, the size of the corroded border is evaluated by exploring the border of the image and evaluating the normal distance to the corrosion edge.

2.2.7. Image treatment – AGC

The global approach involves calibrating corroded glass images against reference images, detecting and quantifying corroded spots, and computing various metrics to assess the extent and severity of corrosion. The code was written in Python with the use of the library skimage.

The initial step involves warping the image to correct for any perspective distortions. Users manually select the four corners of the glass in the image. These selected points are used to define a projective transformation that maps the selected corners to a predefined square grid which corresponds to the glass dimension. This transformation ensures that the image is correctly aligned and scaled, facilitating accurate subsequent analysis. The warping process is as follows:

1. Corner Selection: Users draw lines on the image to mark the four corners of the glass
2. Transformation Definition: A projective transformation is defined using the selected corners and a predefined square grid
3. Image Warping: The transformation is applied to the image, resulting in a warped image that is correctly aligned and scaled

Before further processing, the warped image is converted to grayscale. This transformation simplifies the image by reducing it to a single channel, which is essential for subsequent calibration and spot detection

steps.

The next step in the analysis involves calibrating the corroded glass image using a reference glass image. The calibration process normalizes the corroded image by dividing it by the reference image. Pixels with a ratio below 0.93 are considered corroded and set to zero, while those with a ratio equal to or above 0.93 are considered non-corroded and set to one. This binary calibration helps in distinguishing corroded areas from non-corroded ones.

After calibration, the next step is to detect corroded spots. The calibrated image undergoes morphological closing to connect small bright cracks, which helps in identifying contiguous corroded regions. The connected regions are then labeled, and the area of each region is computed. This process results in a labeled image where each corroded spot is uniquely identified, and a list of corroded spot areas is generated.

Several metrics are then computed to quantify the extent of corrosion:

Total Corroded Area: This metric is calculated by counting the number of corroded pixels in the calibrated image and scaling it to the actual glass area in square millimeters (mm^2).

Corroded Spot Area: The total area of detected corroded spots is computed by summing the areas of all labeled regions and scaling it to the glass area in mm^2.

Spot Density: The density of corroded spots is determined by counting the number of spots larger than a specified minimum area and normalizing it to the glass area in square centimeters (cm^2).

Penetration Depth: The maximum and mean penetration depths are computed for both coated and uncoated sides of the glass. This involves removing a specified number of edge pixels and calculating the profile of the side. The maximum and mean values of this profile are then scaled to the actual side length of the glass. The steps are:

- Edge Removal: Remove a specified number of pixels from the edges to avoid boundary effects.
- Profile Calculation: Sum the pixel values along the depth to get the penetration profile.
- Depth Computation: Calculate the maximum and mean values of the penetration profile and scale them to the actual side length.

2.2.8. Image treatment – LNEG

The code developed by LNEG is written in *Python* using the *OpenCV* library. The captured image Fig. 11a) is processed by first detecting the green zone, shown by the red frame in Fig. 11b), then detecting the inner contours and analyzing the corresponding areas - the contour with the highest area corresponds to the sample contour, shown by the blue frame in Fig. 11c).

A manual detection method was developed: the user, using a mouse, selects the four corners of the image, thus obtaining the image of the sample.

Given that the sample holder cannot be aimed directly at the camera direction, the captured image is distorted - it forms a trapezoid instead of a square, which needs to be corrected in order to obtain a correct detection of the corrosion. The trapezoid is then transformed into a square using the getPerspectiveTransform function followed by warpPerspective, both from the *OpenCV* library - thus obtaining a photograph of the sample that is as close to reality as possible.

As it is not possible to guarantee that both the position of the sample on the holder and its direction are exactly the same in all photos, it is not possible to make a pixel-by-pixel comparison with a reference sample. So, the image needs to be segmented in order to select the objects of interest - the corrosion and the part of the sample without corrosion. Because there are different light conditions inside the same sample, and in order to improve the quality of the detection, the *CLAHE* algorithm for contrast enhancement was used. After that, the image is converted to greyscale and the mean and standard deviation of the pixels in the image are obtained. Using those values, a threshold is calculated, which will be used for creating a mask where the white areas are considered as corrosion and black ones as non-corrosion.

The corrosion is classified as belonging to the edges, which are divided into protected and unprotected edges, according to the user's choice, and can belong to the top, bottom, left and right or as belonging to the center - like the spots. The corrosion detected is identified with different colors, depending on the characteristics described above.

Once the identification of all the corrosion areas detected has been finalized, it is necessary to extract and save data such as maximum and average penetration, both of protected and unprotected edges; area of corrosion on edges; number of spots found, density of spots, area of spots and total area and percentage of corrosion.

2.3. Outdoor exposure campaign

For this study, results from a 68-month lasting outdoor exposure campaign in Tabernas (PSA), (37°, 6′, N; 2°, 21′ W) and Almería (ALM), (36°, 50′ N; 2° 28′ W), both in Spain, are used. The exposure started in 2017 and is still ongoing by 2024. Samples are exposed on racks like it can be seen in Fig. 12. The distance to the ground is between 1.0 and 1.5 m with a horizontal tilt angle of 45°, facing south. To identify the corrosivity of the sites, the corrosivity class is determined according to ISO 9223:2012 [11]. Resulting corrosivity classes for Almería and Tabernas are C3 and C2 (for steel, aluminum and zinc), respectively, meaning Almería exhibits a more corrosive environment than Tabernas. Details regarding the four different materials can be taken from the appendix. Two silvered-glass reflector materials are studied in this campaign: The commercial one (RL1), whose protective back system is composed by three paint layers with a thickness of 28, 33 and 35 μm (for the prime, intermediate and top coats, respectively) and an innovative low-lead reflector (RL3) with two paint layers in which the lead content is negligible (the thickness of the paint layers is 31 and 35 μm). The price of the RL3 reflector is more expensive compared with the commercial RL1. Samples are collected and photos are taken in the laboratory after certain time intervals. Also, the near-normal solar-weighted hemispherical reflectance $\rho_{s,h}$ is measured with a Perkin Elmer Lambda 1050 spectrophotometer equipped with a 150 mm integrating sphere and the near-normal monochromatic specular reflectance $\rho_{\lambda,\varphi}$ is measured with a D&S 15R-USB from Devices and Services. After the characterization in

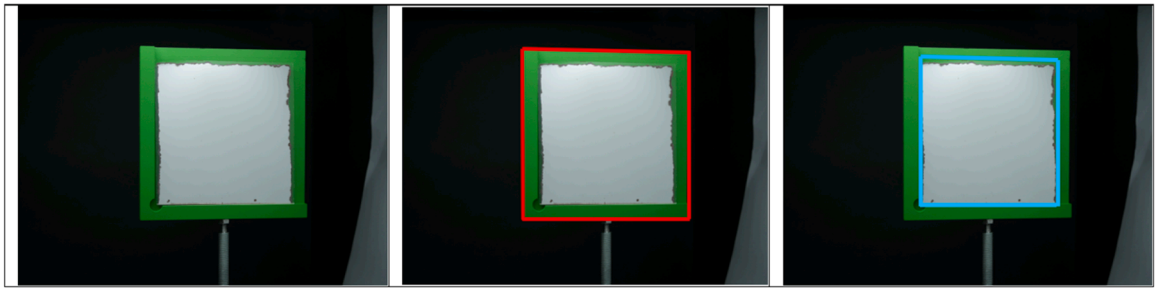

Fig. 11. Steps of image analysis. a) image captured, b) detection of the entire area, shown in red; c) detection of the inner contours shown in blue.

Fig. 12. Outdoor exposure of reflector samples at two different sites: a) Almería and b) Tabernas (PSA, owned by CIEMAT).

the laboratory, the samples are exposed again. Thereby, the evolution of natural aging effects on the same sample can be tracked.

3. Results and discussion

The results of the first-, and the second Round Robin test on image analysis are presented in a consecutive manner. Afterwards, the image-based data from the outdoor exposed samples are discussed and compared with the respective reflectance measurements.

3.1. Results of first Round Robin on corrosion detection

Table 4 displays images of the three investigated samples, along with corresponding treated images from the four participants.

No conventions are established regarding colors, additional scales and markings in the images. While the qualitative comparison of the images looks quite consistent and only minor deviations between the evaluated samples can be seen, the quantitative results, displayed in Fig. 13 exhibit noticeable deviations between the four participants, which are beyond an acceptable level for this analysis method to be of importance for the community. The following three parameters are shown: the total corroded area, corrosion spot area and corrosion spot density. Regarding the total corroded area, it can be said, that all participants find the lowest values (between 347 and 440 mm^2) for sample number two, while samples number 1 and 3 exhibits around values twice as high. For the ranking of the institutes for each sample no trend can be observed. The same lack of ranking trend holds true for the corrosion spot area parameter. All participants detect the largest corrosion spot area for sample number 3 with values between 38 and 73 mm^2, while the corrosion spots on samples number 1 and 2 make up for <20 mm^2. For the third parameter, the corrosion spot density, DLR measures by far the largest values, namely 1.1, 2.7 and 6.6 spots/cm^2 for samples from 1, 2 and 3, respectively. The other three participants measure values not higher than 0.1.

From the absolute values, the coefficient of variation *CV,* i.e., the relative dispersion of data points around the mean of the four participants is provided for each parameter in Table 5. Consensus among the institutes is mostly established for the total corroded area, with *CV* ranging from 11.4 % to 30.3 % across the three samples. Deviations are higher for the evaluation of corrosion spot area, and for spot density. For the latter, OPAC measures values one order of magnitude higher than the other three participants. On average over the three samples the corrosion spot area shows a *CV* of 59.2 % and the parameter of the spot density of 175.0 %. Hence, it can be stated that the total corroded area is determined with acceptable agreement (average *CV* of 18.7 %), but the assignment to single or multiple spots, or edge corrosion lacks consensus. After a discussion of these results among the participating experts, the second Round Robin was performed with the aim to decrease the respective *CV*-values and also implement additional parameters that describe the corrosion on the edges.

3.2. Results of second Round Robin on corrosion detection

After discussing the results from the first Round Robin among the participants, the parameter definitions are specified more precisely and also some new, more reasonable parameters are implemented (see step 6 in Section 2.2.5). With these new conventions, a second batch of five samples is evaluated in a second Round Robin. The raw images of the five samples taken in the OPAC setup are shown in Table 6. The first four samples were selected to represent the typical corrosion effects that are of interest for research. Namely, where a few small spots are forming in the inner part of the reflector and the coated edge which is present on one side of the reflector is corroded in a less pronounced way than the remaining uncoated three edges. In ongoing research, it would be beneficial to thoroughly and mutually identify the progress of corrosion among various institutes to achieve agreement on advancements/failures in sample production. The fifth sample is added as an extreme but still realistic case and benchmark the evaluation procedures also in those cases. The fifth sample does not exhibit a coated edge, all edges are cut.

Similarly, to the first Round Robin, the results from the image analysis of the main corrosion parameters, total corroded area, corrosion spot area and the spot density are shown in Fig. 14. Since corresponding results of the fifth sample lie in a different order of magnitude, they are displayed by the right y-axis. It can be seen that for the total corroded area, the values reported by the participants are in good agreement and follow the same trend for the five samples. The sample order from low to high values is the same for all participants: 1, 4, 2, 3, 5 (for DLR and LNEG sample 2 and 3 are interchanged). The other two parameters (corrosion spot area and spot density) exhibit less agreement between the participants, however a significant improvement in comparison to the first Round Robin is obvious from the graphs. This is especially the case for the spot density, where during the first Round Robin, DLR measures one order of magnitude higher values than all the other participants, this improves in the second Round Robin and the corresponding values of samples 1 – 4 lies between 0.03 and 0.29, while for sample 5 the values vary between 0.28 and 1.83.

Additionally, the penetration of the corrosion is evaluated by the four participants. This parameter is explained in Section 2.2.5 Image treatment - OPAC in step 5. It is differentiated between coated and uncoated edges and the maximum- and mean penetration is evaluated in Fig. 15. Regarding the determined maximum penetration of the coated edge, the institutes find values between 0.8 mm and 3.4 mm. On sample 1, 2 and 3 the highest value is always measured by LNEG. Regarding the uncoated penetration maximum, the values lie closer together and also a similar trend can be observed regarding the ranking of the five sample. Regarding the mean values of the coated edges it can be observed that the range of the calculated values is between 0.4 mm and 1.2 mm and while OPAC and AGC always measure lower values than CEA and LNEG

Table 4
images from first Round Robin, each column represents one sample, the first row shows the raw images from OPAC, while the following rows represent the evaluated samples from OPAC, AGC, CEA and LNEG, respectively.

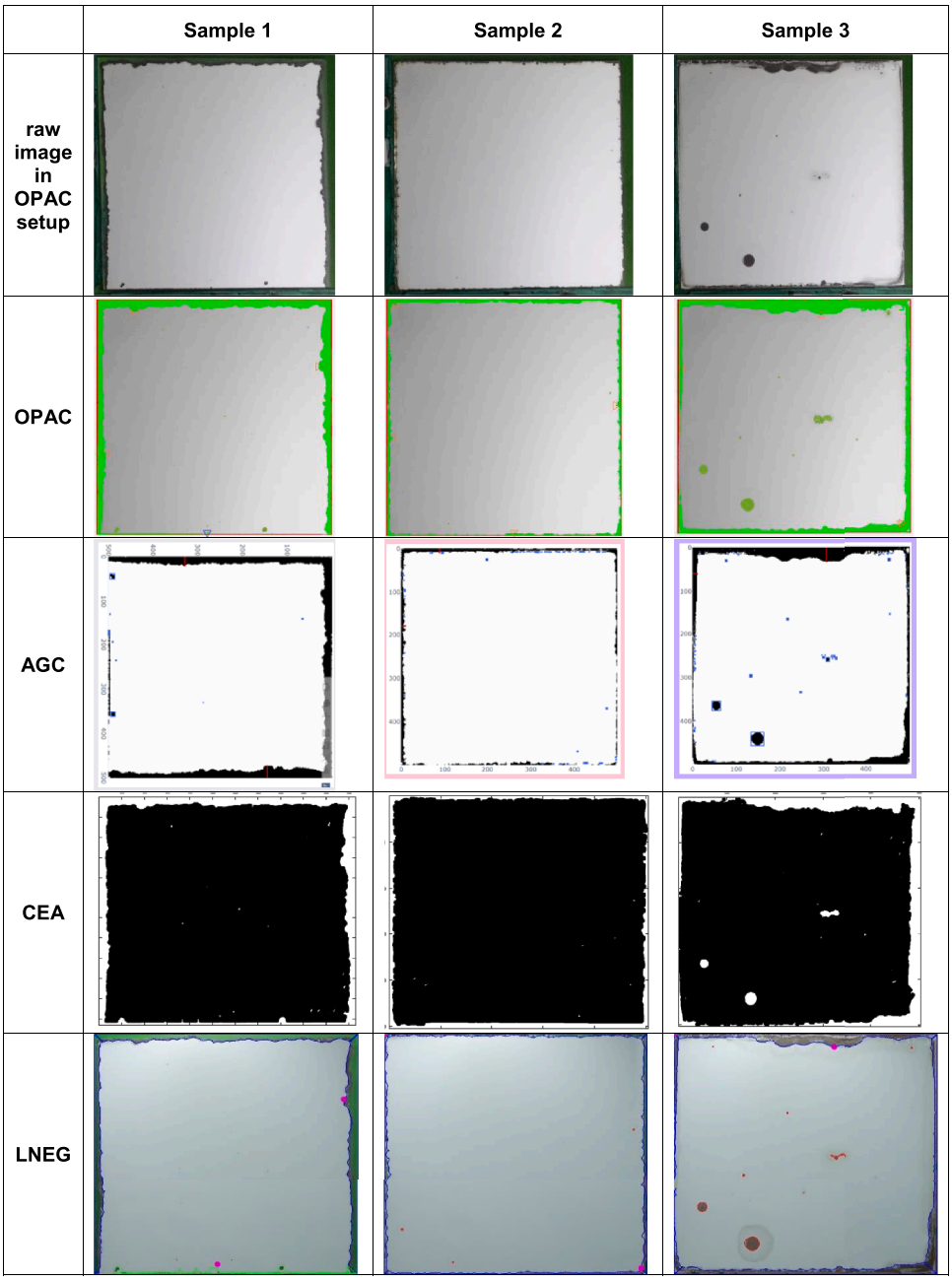

for samples 1, 2 and 3, this trend is reversed for sample number 4. Similarly, to the uncoated penetration maximum, a clear trend can be observed for the uncoated penetration mean values, which translates into a ranking from low to high penetration mean values for the sample order 1, 5, 4, 3 and 2. This trend is found almost exactly by all participants, making the uncoated penetration mean and maximum values to practical parameters of comparison. What also shall be mentioned here is the obvious disadvantage regarding corrosion formation of the uncoated edges over the coated edges. The two upper graphs a) and b) which represent the coated edges are continuously measured to exhibit less corroded area compared to the coated edges in the bottom graphs c) and d). The mean values over the four participants of the penetration on the uncoated edges is increased by a factor of 1.3, 4.0, 3.7 and 1.9 compared to the coated edges of sample 1, 2, 3 and 4, respectively.

The coefficient of variation *CV* for the different parameters and samples are calculated and are shown in Table 7. It can be noted that in comparison to the first Round Robin, the average *CV* values improved. For the total corrosion area, the average value of the five samples is calculated to 14.3 %. The average values of the other two parameters, corrosion spot area and spot density decreased significantly to 35.8 % and 62.6 %. Therefore, the agreement between the four participants regarding these parameters is now around twice as good as during the first Round Robin. Interestingly, no trend can be observed for this evaluation regarding the agreement among the participants. For example, the lowest *CV* values, and therefore the best agreement, can be noted on sample 5 for the parameters of total corrosion area (6.0 %) and the corrosion spot area (15.1 %), while the parameter spot density (95.4 %) shows the worst agreement on this sample. Furthermore, the highest

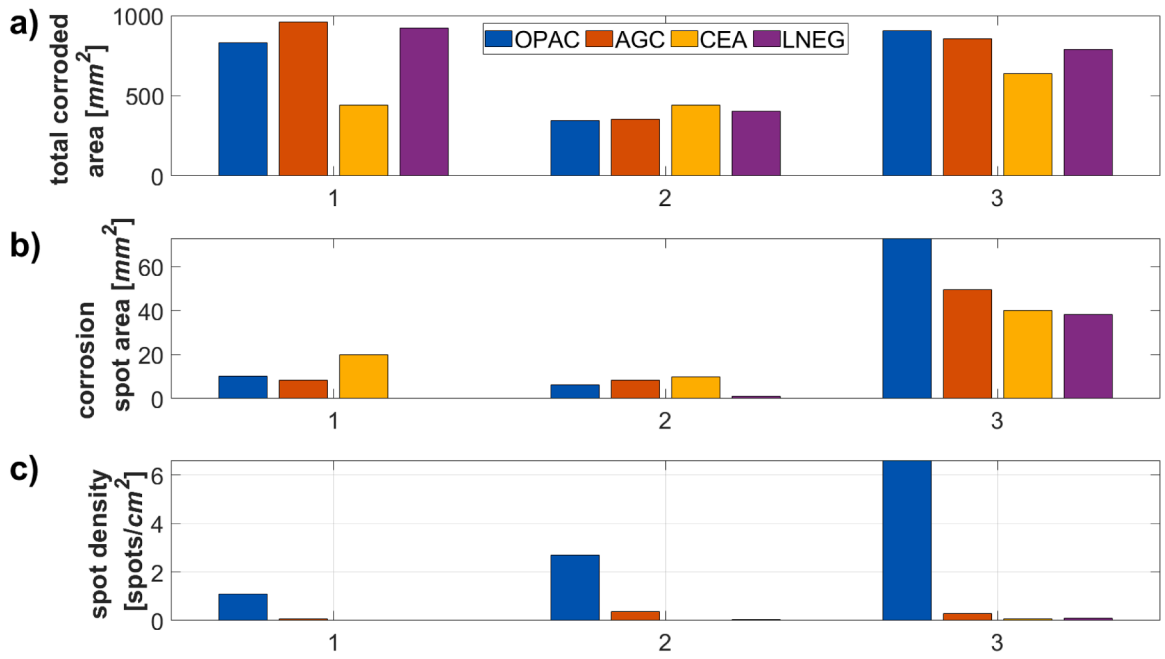

Fig. 13. Corrosion parameters obtained by the four participants for the three samples, from left to right: the total corroded area, the corrosion spot area and the spot density.

Table 5
Coefficient of variation *CV* referred to the corresponding mean values for the respective parameters for each sample, and the average of all three samples.

%	1	2	3	AVERAGE
TOTAL CORROSION AREA	30.3	11.4	14.4	**18.7**
CORROSION SPOT AREA	84.8	61.1	31.7	**59.2**
SPOT DENSITY	175.9	166.1	183.1	**175.0**

CV value, and therefore the worst agreement on the total corrosion area is measured for sample 1 (24.5 %) while this sample shows the lowest *CV* value for the spot density (32.0 %).

Regarding the edges, it can be seen that the spreading of the maximum penetration values is higher than the mean values for the coated edge, while for the uncoated edges it is the other way around. Also, it can be noted, that the agreement is better for the uncoated edges, both on maximum and mean penetration. The maximum deviation can be detected for sample number 3 with a *CV* of 72.7 % regarding the coated maximum penetration, and the best agreement is found for sample 1 where the *CV* of the uncoated penetration maximum is 8.8 %. No systematic error can be seen in the data since there is no permanent outlier for any participant. It shall be noted that the parameter of the uncoated penetration maximum exhibits the lowest *CV* average value of 13.4 % and can therefore be regarded as the most promising one for reliable comparative studies among different institutes.

If these absolute values of deviations on the inter-institute level are tolerable certainly depends on the demands of the respective application. It is worthwhile to mention the study realized by Smestad et al. [23] found very comparable coefficients of variation in their Round Robin based on image analysis of soiled reflectors. Taking especially into account the simplicity of data acquisition, the participating experts assess the developed technique as useful and plan on further using it during their upcoming projects. In order to further increase the agreement between participants a centralized image taking process, or standardized photo box would probably make the largest impact.

3.3. Corrosion evaluation on outdoor exposed samples

The progression of the overall corroded area for both sample types at outdoor locations over specific time intervals is evaluated by the OPAC laboratory and depicted in Fig. 16. The first data point is measured after 24 months and while the RL1 sample at the C2 site exhibits an area of 40 mm², the RL3 sample at the C3 site already lost 651 mm² of its reflective area due to corrosion. Notably, a consistent upward trend is observed over the exposure period, except for an outlier in the RL3 sample at the C2 spot after 48 months. This anomaly can be attributed to incorrect illumination conditions during the photographing process. This upward trend can be explained by the continuous corrosion of the silver layer of the reflectors, especially on the uncoated edges (see Fig. 17b). However, this trend is different for the two sites. For the C2 site, the total corroded area for the samples RL1 and RL3 increases from 40 mm² to 59 mm² and from 229 mm² to 280 mm² over the period between 24 and 68 months, respectively. In relative terms, it corresponds to 47.5 % and 22.2 %. For the C3 site however, the respective area increases for the RL1 and RL3 samples are from 240 mm² to 426 mm² and from 651 mm² to 1308 mm², which relates to a relative increase of 77.5 % and 100.9 %. Hence, the advancing of the corrosion effect is faster at the C3 site than at the C2 site. Another two key observations emerge from the data: firstly, a significant disparity in the total corroded area between RL1 and RL3 sample types. The RL3 samples consistently exhibit double to fivefold higher corrosion areas compared to RL1 samples, suggesting that the commercial layer structure of RL1 samples is more corrosion resistant than the innovative paint composition of the RL3 sample. Secondly, the results align with corrosivity class determination, as the total corroded area at the C3 site is approximately five times larger than at the C2 site after the same exposure period for both sample types. This underscores the value of identifying the corrosivity class of a site for a solar power plant in order to thoroughly determine reflector requirements. It shall further be emphasized that the evaluation qualifies the developed image-based analysis technique, since the conclusions are justified even when the respective inaccuracy is taken into consideration. Also to mention that similar results were obtained Buendía-Martínez et al. [29], but with unknown error margins, which can now be reported because of the performed Round Robin experiment.

Table 6
raw images of second Round Robin samples from OPAC setup.

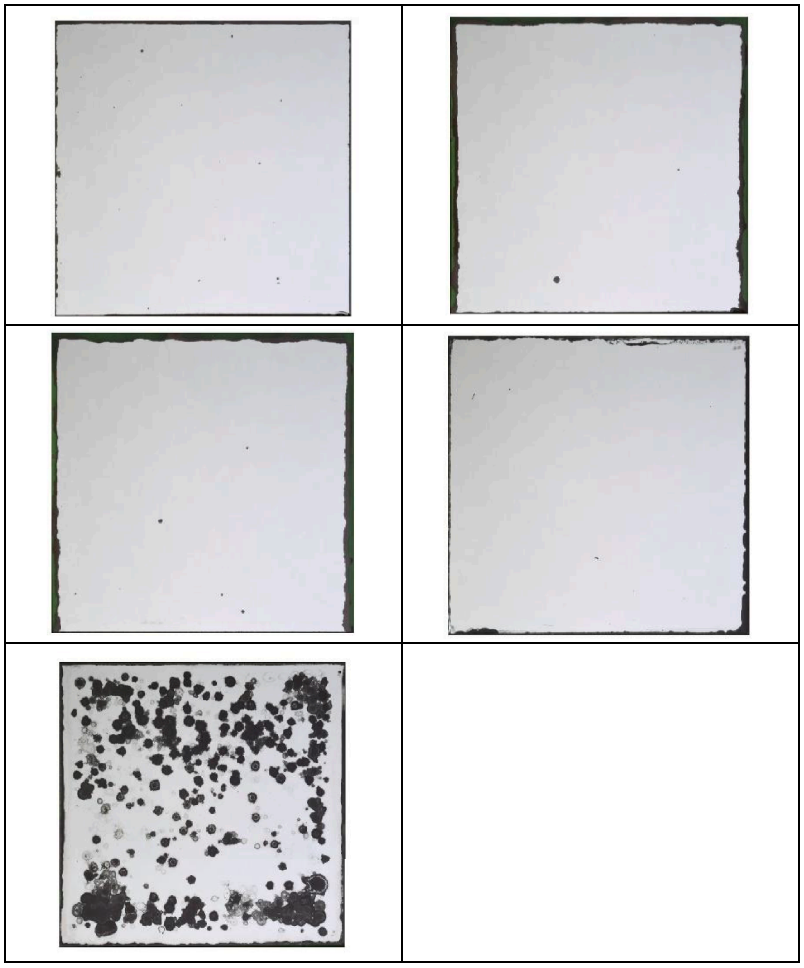

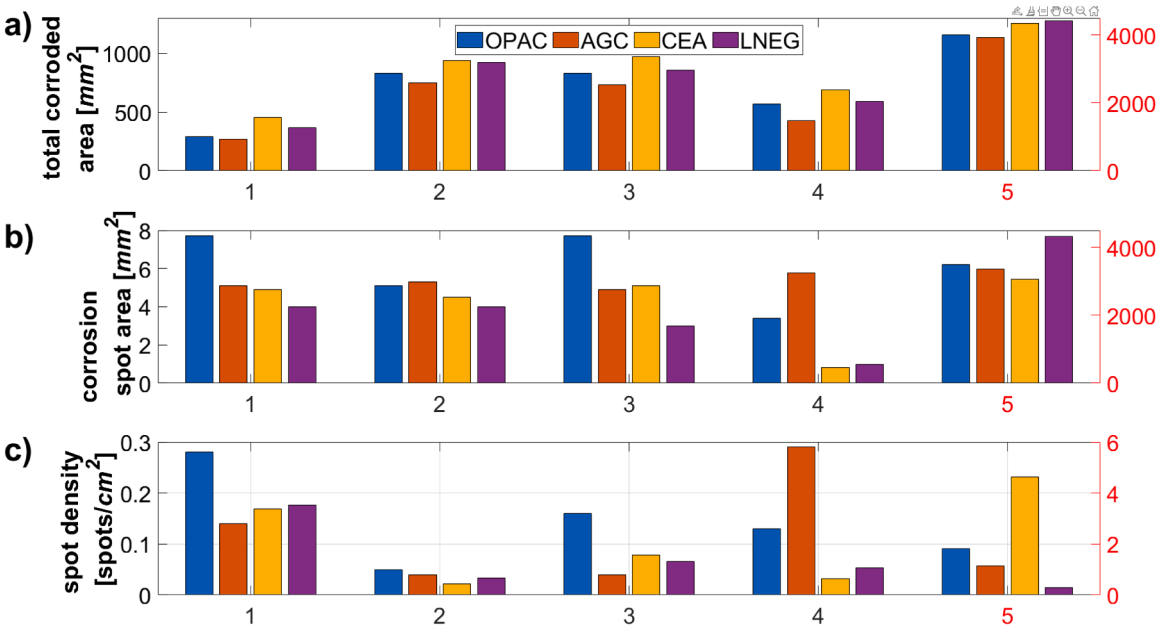

Fig. 14. a) total corroded area, b) corrosion spot area and c) spot density for the five evaluated samples of the second Round Robin test among the four participants OPAC, AGC, CEA and LNEG. Data from the fifth sample correspond to the right y-axis.

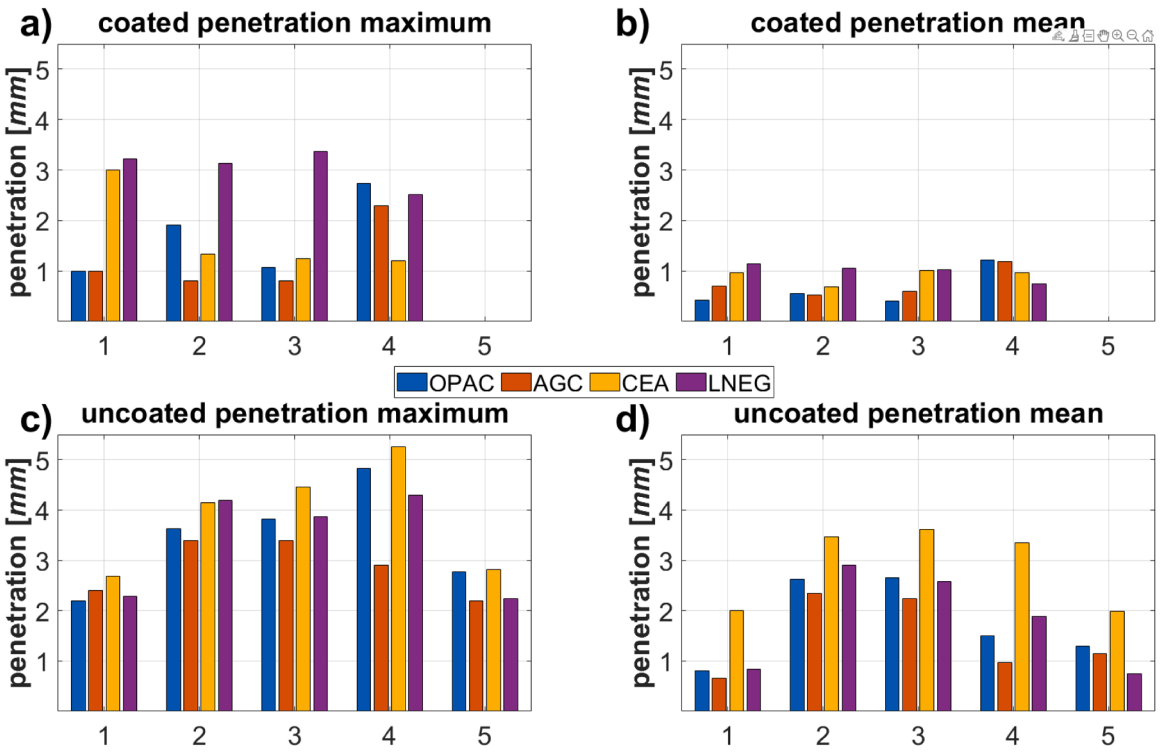

Fig. 15. Comparison of the evaluation of the corrosion penetration on the coated (upper graphs) and uncoated (bottom graphs). Left side graphs depict the maximum penetration and right side graphs the mean penetration.

Table 7
Coefficient of variation *CV* for the respective parameters for each sample, and the average of all five samples.

%	1	2	3	4	5	AVERAGE
TOTAL CORROSION AREA	24.5	10.4	11.7	19.0	6.0	**14.3**
CORROSION SPOT AREA	29.3	12.5	37.3	84.9	15.1	**35.8**
SPOT DENSITY	32.0	32.5	60.3	92.7	95.4	**62.6**
COATED PENETRATION MAXIMUM	59.4	56.3	72.7	31.2	–	**54.9**
COATED PENETRATION MEAN	39.1	34.4	41.1	21.6	–	**34.0**
UNCOATED PENETRATION MAXIMUM	8.8	10.2	11.2	23.7	13.2	**13.4**
UNCOATED PENETRATION MEAN	34.2	12.7	12.8	32.1	29.8	**24.3**

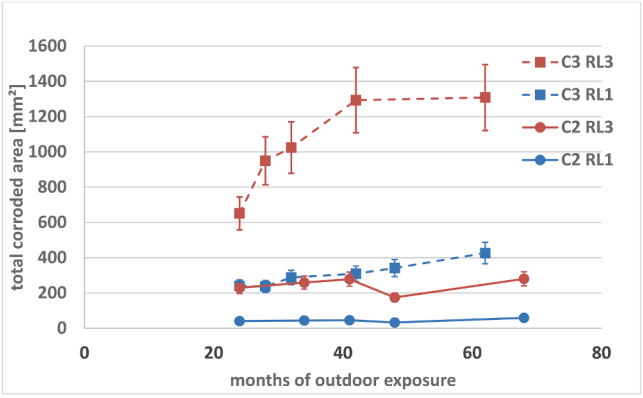

Fig. 16. Evolution of the total corroded area for the two sample types RL1 and RL3 at two outdoor exposure spots with different corrosivity classes C2 and C3 over up to 68 months. The error bars reflect the CV value during the Round Robin experiment from given in Table 7.

Notably, no instances of inner corrosion spots are detected in the investigated samples, and therefore, this parameter is not presented. However, some other samples on the C3 site exhibit corrosion spots on both sample types. Unfortunately, due to insufficient tracking of those specific samples over time, the temporal evolution of the spots cannot be illustrated. Additionally, a noteworthy observation pertains to the coated edges. Corrosion detected on these edges is significantly lower than on the cut edges. This is illustrated in Fig. 17 which shows photos of the RL3 sample in its initial state, after 68 months of outdoor exposure to a C2 site and the resulting image after the application of the DECORI code at OPAC. The different behavior of edge characteristics towards corrosion is demonstrated for the artificially aged samples before, and is confirmed during the outdoor exposure testing. The uncoated penetration mean value for this sample was determined to 0.5 mm, while the coated edge, in this picture the upper one, does not exhibit any significant penetration.

The reflectance measurements of $\rho_{s,h}$ and $\rho_{\lambda,\varphi}$ which are performed on these four reflectors after the latest sample recovery of the outdoor exposure campaign are given as reflectance loss referred to their respective initial values. It can be observed that both reflectance values remain either stable or decrease only with values between 0.001 and 0.005, which can be regarded as a small decrease during this long outdoor exposure. However, it is neither possible to conclude from these measurements that the C3 exhibits a higher corrosivity than the C2 site, nor that the RL1 coating clearly outperforms the RL3 coating with respect to its corrosion resistance. Those two findings could only be made after much longer outdoor exposure campaigns as long as the characterization would only be based on state-of-the-art reflectometer measurements, namely when the measurement spot of the respective instrument would be aligned on a corroded area.

Table 8

4. Conclusion

The first Round Robin is used to shed light on the general feasibility

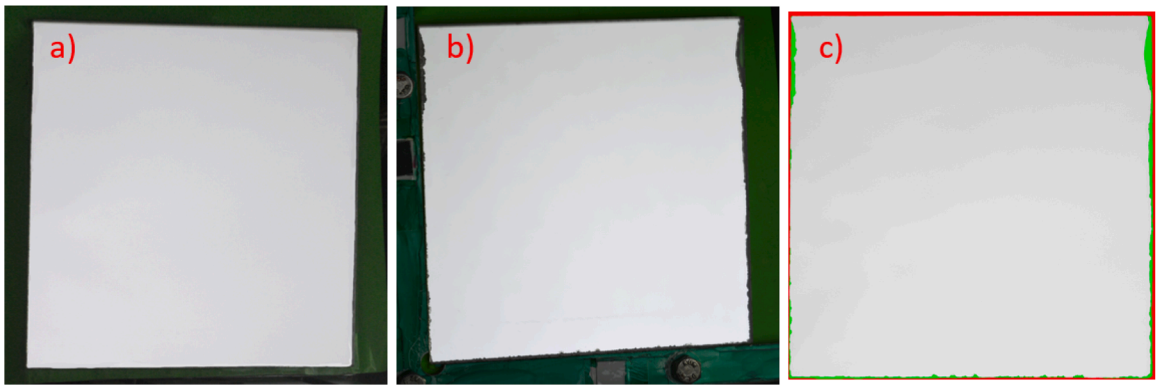

Fig. 17. Illustration of the difference between original edge and unprotected edge of RL3 sample: a) in initial state; b) after 68 months of exposure to C2 site and c) image treatment result with color markings: red stands for artefact due to perspective and shadow formation, which is especially the case for the original coated, upper edge, while green corresponds to the actual corrosion area.

Table 8
Measured reflectance losses after the maximum duration of the outdoor exposure campaign.

	$\Delta\rho_{s,h}$			$\Delta\rho_{\lambda,\phi}$		
C3 RL3	−0.002	±	0.001	−0.004	±	0.001
C3 RL1	−0.002	±	0.001	−0.002	±	0.001
C2 RL3	0.000	±	0.000	−0.001	±	0.002
C2 RL1	−0.001	±	0.000	−0.005	±	0.001

and ensure the development of an unbiased approach to realize this technique at each participating laboratory. During the second Round Robin, mutually agreed on corrosion parameters like the total corrosion area, the corrosion spot density, the edge corrosion penetration etc. are thoroughly defined and are measured on five reflector samples that are send to the four participants. The comparison of the data among the institutes lead to coefficients of variation between 62.6 % and 13.4 %. Also, since these values are in line with literature [23] it is assessed by the experts, that they justify the usage of the technique in further projects. On the one hand, since it gives valuable insights in coating performance which could not be achieved by traditional reflectometer measurements and on the other hand can be implemented in laboratories without expensive instrumentation or complex procedures. With the coefficients of variation values detected in this work, future studies benefit from well-defined error margins when their results shall be compared to other institutes. Thereby the here presented image-based methodology might gain more popularity since its trustworthiness and accuracy is more substantiated. It is particularly valuable when the entire sample needs to be characterized rather than isolated microscopic areas, for example, to quantify advancing corrosion phenomena. One noticed limitation of the methodology is human failure when the coated edge is to be detected by human eye in the image, especially in those cases, where there is only very few edge corrosion present. The developed methodology is already in use at the OPAC laboratory and forms part of the continuous sample characterization procedure during running projects, dealing with the stability of novel coating composition types.

The developed analysis technique is further applied to samples from a 68-months lasting outdoor exposure campaign where two different reflector coatings are exposed at two sites of different corrosivity. Through the determination of the total corroded area several conclusions can be made: firstly, that the site which exhibits a C3 corrosivity level (according to ISO9223) has stronger effects on the coating than the site with C2 corrosivity level. This statement can be made because the measured total corroded area for the C2 site for the samples RL1 and RL3 increases from 40 mm^2 to 59 mm^2 and from 229 mm^2 to 280 mm^2 over the period between 24 and 68 months, respectively. For the C3 site however, the respective area increases for the RL1 and RL3 samples are from 240 mm^2 to 426 mm^2 and from 651 mm^2 to 1308 mm^2, thus showing higher absolute values and also higher relative increase than on the C2 site.

Secondly, that the commercial RL1 coating exhibits a higher corrosion resistance than the novel RL3 coating. This can be seen when the total corroded area after the exposure campaign is compared. On the commercial coating RL1, a total corroded area of 59 mm^2 and 426 mm^2 is measured after the outdoor exposure on the C2 and the C3 site, respectively, while on the novel low-lead coated reflector RL3 corresponding values are 280 mm^2 and 1308 mm^2.

And thirdly, from the inspection of the corrosion penetration on the edges of the sample it clearly becomes obvious that a cut edge on a sample presents an efficient gateway for edge corrosion while the original coated edge is not affected by corrosion at the exposure sites used in this study.

It shall be emphasized that state of the art reflectance measurements of $\rho_{s,h}$ and $\rho_{\lambda,\varphi}$ which are performed before and after the exposure lead to only negligible reflectance losses between 0.000 and 0.005. Hence, not permitting any of the three conclusions that are made by the novel image-based technique. This demonstrates the additional value of the here presented image analysis technique for solar reflector qualification.

CRediT authorship contribution statement

Florian Wiesinger: Writing – review & editing, Writing – original draft, Visualization, Validation, Supervision, Software, Methodology, Investigation, Formal analysis, Data curation, Conceptualization. **Sarah Baghouil:** Writing – original draft, Software, Methodology, Investigation. **Estelle Le Baron:** Writing – review & editing, Software, Methodology, Investigation, Funding acquisition. **Romain Collignon:** Software, Methodology, Investigation. **Filipa Santos:** Writing – original draft, Software, Methodology, Investigation. **Teresa C. Diamantino:** Writing – review & editing, Writing – original draft, Software, Methodology, Investigation, Funding acquisition. **Isabel Catarino:** Software, Methodology, Investigation. **Jorge Facão:** Software, Methodology, Investigation. **Cristina Ferreira:** Software, Methodology, Investigation. **Soraia Páscoa:** Software, Methodology, Investigation. **Florian Sutter:** Supervision, Project administration, Funding acquisition. **Aránzazu Fernández-García:** Supervision, Funding acquisition. **Johannes Wette:** Writing – review & editing, Investigation, Formal analysis.

Declaration of competing interest

The authors declare that they have no known competing financial interests or personal relationships that could have appeared to influence the work reported in this paper.

Acknowledgments

The results in this publication were produced within the GreenCoat project (project number 03EE5066A), supported by the Federal Ministry of Economic Affairs and Climate Action (BMWK), based on a resolution of the German Parliament.

Gefördert durch:

Bundesministerium für Wirtschaft und Energie

aufgrund eines Beschlusses des Deutschen Bundestages

Supplementary materials

Supplementary material associated with this article can be found, in the online version, at doi:10.1016/j.rineng.2024.103781.

Appendix

Table 9

Table 9
Details of the evaluation of the corrosivity class of the Almeria and Tabernas site regarding the exposed metal coupons and their corresponding classification.

Site/Material	Steel	Copper	Aluminum	Zinc	**Average**
Almeria	C3	C5	C3	C3	**C4**
Tabernas	C2	C4	C2	C2	**C3**

Data availability

Data will be made available on request.

References

[1] I.R.E. Agency (IRENA), Renewable Energy technologies: Cost analysis Series, 1, International Renewable Energy Agency (IRENA), 2012, p. 274.
[2] A. Fernández-García, M.E. Cantos-Soto, M. Röger, C. Wieckert, C. Hutter, L. Martínez-Arcos, Durability of solar reflector materials for secondary concentrators used in CSP systems, Solar Energy Materials and Solar Cells 130 (2014) 51–63, https://doi.org/10.1016/j.solmat.2014.06.043.
[3] F. Sutter, Y. Binyamin, T. Zoschke, A. Fernández-García, S. Naamane, M. Galetz, R. Reoyo-Prats, F.J. Pérez-Trujillo, A. Aglüro, F. Orioli, J. Piron, D. Mandler, A. Attout, S. Caron, J. Wette, R. Sánchez, A. Morales, C. Hildebrant, RAISELIFE project extends the lifetime of functional CSP materials, AIP. Conf. Proc. 2445 (2022) 020013, https://doi.org/10.1063/5.0085763.
[4] C.E. Kennedy, K. Terwilliger, Optical durability of candidate solar reflectors, J. Sol. Energy Eng. 127 (2005) 262–269.
[5] C.N. Njoku, B.N. Enendu, S.J. Okechukwu, N. Igboko, S.O. Anyikwa, A.I. Ikeuba, I. B. Onyeachu, I.I.N. Etim, D.I. Njoku, Review on anti-corrosion properties of expired antihypertensive drugs as benign corrosion inhibitors for metallic materials in various environments, Results. Eng. 18 (2023) 101183, https://doi.org/10.1016/j.rineng.2023.101183.
[6] P. Palenzuela, D.C. Alarcón-Padilla, G. Zaragoza, Large-scale solar desalination by combination with CSP: Techno-economic analysis of different options for the Mediterranean Sea and the Arabian Gulf, Desalination. 366 (2015) 130–138, https://doi.org/10.1016/j.desal.2014.12.037.
[7] Z.M. Omara, W.H. Alawee, A. Basem, A.D. Jawad Al-Bayati, Heat loss reduction techniques for walls in solar stills: A review, Results. Eng. 22 (2024) 101996, https://doi.org/10.1016/j.rineng.2024.101996.
[8] F. Sutter, A. Fernandez-García, J. Wette, P. Heller, Comparison and Evaluation of Accelerated Aging Tests for Reflectors, Energy Procedia 49 (2014) 1718–1727, https://doi.org/10.1016/j.egypro.2014.03.181.
[9] A.P. Gonzalo, A.P. Marugán, F.P.G. Márquez, A review of the application performances of concentrated solar power systems, Appl. Energy 255 (2019) 113893.
[10] R. Schemenauer, H. Fuenzalida, P. Cereceda, A Neglected Water Resource: The Camanchaca of South America, Bull. Am. Meteorol. Soc. 69 (1988) 138–147, https://doi.org/10.1175/1520-0477(1988)069<0138:ANWRTC>2.0.CO;2.
[11] ISO 9223, Corrosion of Metals and Alloys - Corrosivity of Atmospheres - Classification, determination and Estimation, International Organization for Standadization, 2012 n.d.
[12] K. Slamova, Mapping atmospheric corrosion in coastal regions: methods and results, J. Photon. Energy 2 (2012) 022003, https://doi.org/10.1117/1.JPE.2.022003.
[13] E. Schindelholz, Comparability and accuracy of time of wetness sensing methods relevant for atmospheric corrosion, Corros. Sci. (2013) 9.
[14] F. Corvo, N. Betancourt, A. Mendoza, The influence of airborne salinity on the atmospheric corrosion of steel, Corros. Sci. 37 (1995) 1889–1901, https://doi.org/10.1016/0010-938X(95)00058-R.
[15] F. Buendía-Martínez, F. Sutter, J. Wette, L. Valenzuela, A. Fernández-García, Lifetime prediction model of reflector materials for concentrating solar thermal energies in corrosive environments, Solar Energy Materials and Solar Cells 224 (2021) 110996, https://doi.org/10.1016/j.solmat.2021.110996.
[16] RAFAEL ALMANZA, C.H.E.N. JIEFENG, GENARO CORREA, MARCOS MAZARI, FURTHER OPTION FOR SOLAR CONCENTRATORS: ALUMINUM FIRST SURFACE MIRRORS, Solar Energy (1995).
[17] A. Fernandez-Garcia, F. Sutter, M. Montecchi, F. Sallaberry, A. Heimath, C. Heras, E. Le Baron, A. Soum-Glaude, Parameters and Method to Evaluate the Reflectance Properties of Reflector Materials for Concentrating Solar Power Technology Technology - Official Reflectance Guideline Version 3.1, SolarPACES, 2020.
[18] A. Fernández-García, F. Sutter, L. Martínez-Arcos, C. Sansom, F. Wolfertstetter, C. Delord, Equipment and methods for measuring reflectance of concentrating solar reflector materials, Solar Energy Materials and Solar Cells 167 (2017) 28–52, https://doi.org/10.1016/j.solmat.2017.03.036.
[19] C. Sansom, A. Fernández-García, P. King, F. Sutter, A. García-Segura, Reflectometer comparison for assessment of back-silvered glass solar mirrors, Solar Energy 155 (2017) 496–505, https://doi.org/10.1016/j.solener.2017.06.053.
[20] M. Khayatazad, L. De Pue, W. De Waele, Detection of corrosion on steel structures using automated image processing, Developments in the Built Environment 3 (2020) 100022, https://doi.org/10.1016/j.dibe.2020.100022.
[21] A.R.M. Forkan, Y.B. Kang, P.P. Jayaraman, K. Liao, R. Kaul, G. Morgan, R. Ranjan, S. Sinha, CorrDetector: A framework for structural corrosion detection from drone images using ensemble deep learning, Expert. Syst. Appl. 193 (2022) 116461, https://doi.org/10.1016/j.eswa.2021.116461.
[22] C. Cai, L. Zhang, J. Zhou, L. Zhou, Sky images based photovoltaic power forecasting: A novel approach with optimized VMD and Vision Mamba, Results. Eng. 24 (2024) 103022, https://doi.org/10.1016/j.rineng.2024.103022.
[23] G.P. Smestad, C. Anderson, M.E. Cholette, P. Fuke, A.A. Hachicha, A. Kottantharayil, K. Ilse, M. Karim, M.Z. Khan, H. Merkle, D.C. Miller, J. M. Newkirk, G. Picotti, F. Wiesinger, G. Willers, L. Micheli, Variability and associated uncertainty in image analysis for soiling characterization in solar energy systems, Solar Energy Materials and Solar Cells 259 (2023) 112437, https://doi.org/10.1016/j.solmat.2023.112437.
[24] L. Micheli, G.P. Smestad, M. Zahid Khan, K. Lange, H.M.I. Almughary, M. Abraim, Y. Alamat, C.B. Anderson, S. Bentouba, B. Figgis, P. Fuke, A.A. Hachicha, M. Karim, A. Kottantharayil, A.A. Martinez-Morales, A.A. Merrouni, D. Olivares, G. Picotti, J. Rabanal-Arabach, F. Wiesinger, K. Ilse, Soiling in Solar Energy Systems: The Role of the Thresholding Method in Image Analysis, Sol. RRL. (2023), https://doi.org/10.1002/solr.202300654 n/a.
[25] A. García-Segura, A. Fernández-García, M.J. Ariza, F. Sutter, P. Watermeyer, M. Schmücker, L. Valenzuela, Corrosion on silvered-glass solar reflectors exposed to accelerated aging tests with polluting gases: A microscopic study, Corros. Sci. 176 (2020) 108928, https://doi.org/10.1016/j.corsci.2020.108928.
[26] F. Sutter, T.J. Reche-Navarro, G.S. Vicente, A. Fernández-García, Durability of anti-reflective coatings for parabolic trough receivers, in: 2020. https://doi.org/10.1063/5.0028751.

[27] F. Buendía-Martínez, A. Fernández-García, F. Sutter, J. Wette, L. Valenzuela, ENSAYOS DE ENVEJECIMIENTO ACELERADO DE REFLECTORES SOLARES SOMETIDOS A RADIACIÓN UV Y CORROSIÓN, (2020). https://doi.org/10.34637/CIES2020.1.2036.

[28] F. Sutter, A. Fernández, P. Heller, C. Kennedy, S. Meyen, R. Pitz-Paal, M. Schmücker, A new method to characterize degradation of first surface aluminum reflectors, in: 2010.

[29] F. Buendía-Martínez, F. Sutter, J. Wette, L. Valenzuela, A. Fernández-García, Lifetime prediction model of reflector materials for concentrating solar thermal energies in corrosive environments, Solar Energy Materials and Solar Cells 224 (2021) 110996, https://doi.org/10.1016/j.solmat.2021.110996.